Dalton Transactions

Accepted Manuscript

ROYAL SOCIETY OF CHEMISTRY

www.rsc.org/dalton

Cite this: DOI: 10.1039/c0xx00000x

www.rsc.org/xxxxxx

ARTICLE TYPE

Influence of Bi^{3+}-doping on Magnetic and Mössbauer Properties of Spinel Cobalt Ferrite

Shyam K. Gore,[a, b] Rajaram S. Mane, [a,*] Mu. Naushad,[c] Santosh S. Jadhav,[b] Manohar K. Zate,[a] Z. A. Alothman,[c]

Biz K. N. Hui,[d, *]

The influence of Bi^{3+}-doping on the magnetic and the Mossbauer properties of cobalt ferrite ($CoFe_2O_4$), where Fe^{3+} ions are replaced by Bi^{3+} ions for $CoBi_xFe_{2-x}O_4$ ferrites where x = 0.0, 0.05, 0.1, 0.15 and 0.2, has been investigated. The structural and morphological properties of undoped and doped ferrites, synthesized chemically through self ignited sol-gel method, are initially screened using X-ray diffraction, scanning electron microscopy and Fourier transform infrared spectroscopy measurements. The changes in magnetic moment of ions, their coupling with neighboring ions and also cation exchange interaction are confirmed from Mossbauer spectroscopy analysis. The effect of Bi^{3+}-doping on the magnetic properties of $CoFe_2O_4$ ferrite is examined from the vibrating sample magnetometry spectra. Saturation magnetization and coercivity values are initially increased and then decreased with Bi^{3+}-doping. Obtained results with improved saturation magnetization (from 26.36 to 44.96 emu g^{-1}), coercivity (from 1457 to 1863 Oe) and remanence magnetization (from 14.48 to 24.63 emu g^{-1}) on 0.1-0.15 mol Bi^{3+}-doping of $CoBi_xFe_{2-x}O_4$ demonstrate their usefulness in magnetic recording and memory devices.

1. Introduction

Magnetic particles have attracted considerable research interest in recent years due their wide range of applications in magnetic recording, microwave absorption, contrast agent, oxygen evolution, and energy storage devices.[1-5] The materials research dealing with structural, chemical and physical properties belonging to the spinel type structure with general chemical formula $M^{2+}O.M_2^{3+}O_3$ where M^{2+} = Co, Ni, Zn, Cu, Fe and M^{3+} = Al, Cr, Mn, Fe, V etc., is at the front line. The spinels occur as natural minerals[6] few examples of spinels with striking features include $MgAl_2O_4$, $FeAl_2O_4$, Fe_3O_4 etc. The spinel with the metal ion Fe^{3+} present in largest mole-wise concentration is ferrite, generally demonstrates ferrimagnetic nature. The structure and crystal chemistry of spinels have comprehensively been addressed in the literature.[7] The unit cell of spinel structure contains thirty-two closely packed oxygen atoms. The oxygen form a face centered, cubic close packed structure where eight cation occupy tetrahedral A-site and sixteen octahedral site.[8] The occupancy of cation depends on the ionic radii, sizes of interstices, temperature, valency, and electrostatic energy.[9] In ferrite, Fe^{3+} ions control the magnetic characteristics by fluctuating their appearance as divalent (Fe^{2+}) or trivalent (Fe^{3+}) ions. For special applications as like the case where large magnetic moment is needed, the divalent ions substitute for Fe^{3+} ions. The substitution of trivalent ions such as Cr^{3+}, Al^{3+}, Gd^{3+}, Ce^{3+} for Fe^{3+} are generally used in either magnetic or electrical applications.[10-13]

[a]School of Physical Sciences, Swami Ramanand Teerth Marathwada University Nanded-431606, India (EmaiL: rsmane_2000@yahoo.com, Ph.: +919850331971, Fax.: +912462229574), [b]Dnyanopasak Shikshan Mandal's Arts, Commerce and Science College Jintur-431509, India, [c]Advanced Materials Research Chair, Department of Chemistry, College of Science, Bld#5, King Saud University, Riyadh, Saudi Arabia, [d]School of Materials Science and Engineering, Pusan National University, Busan 609-735, Republic of Korea.

In spinel ferrite, an additional non-magnetic ions such as Al^{3+} on octahedral site reduces saturation magnetization by increasing the resistivity.[14] The magnetic and dielectric properties of these ferrites depend upon cation distribution and the exchange interaction among the cations in the two sub-lattices. The octahedral sites are larger than tetrahedral sites. Therefore, ions of smaller ionic radii can enter into tetrahedral site and larger ions enter into octahedral site. Some exceptions are found for Zn^{2+}, Cd^{2+} having larger ionic radius compared to Fe^{3+} ions enter into octahedral site. More easily diamagnetic In^{3+} of higher ionic radius enters the tetrahedral A- site by replacing Fe^{3+} in spinel ferrite.[15-17] Among the different spinel ferrite, cobalt ferrite pay special attention because recently it have been intensively investigated for magnetortheological behavior for smart material,[18] photoluminescence properties,[19] microwave absorbing properties[20] and superparamagnetic properties.[21] Cobalt ferrite ($CoFe_2O_4$) is versatile hard ferrite of wide range of applications in various fields due to its strong magneto-crystalline anisotropy,[22] high coercivity,[23] high saturation magnetization,[24] and chemical stability.[25] Synthesis and magnetic properties of Cd, Mg, Zn, and Al, etc.,-doped ferrites are reported in literature.[26-29] It is anticipated that Bi^{3+} can also enter into both tetrahedral and octahedral sites by forming $CoBi_xFe_{2-x}O_4$. Replacing Fe^{3+} with Bi^{3+} would be fascinating because Bi^{3+} is non-magnetic which can promote the saturation magnetization and can reduce the magnetic anisotropy.[30]

In this paper, we report synthesis of Bi^{3+}-doped $CoFe_2O_4$ ferrites using sol-gel self combustion method. Changes in structural, morphological, magnetic and Mossbauer properties of $CoFe_2O_4$ on Bi^{3+}-doping, in place of Fe^{3+}, are investigated. Bi^{3+}-doping influences significantly on the magnetic properties of $CoFe_2O_4$ by varying value of saturation magnetization (M_s), coercivity (H_c), remanence magnetization (M_r) and remanence ratio (R) etc.

2. Experimental details

The synthesis of $CoBi_xFe_{2-x}O_4$ ($0 \le x \le 0.2$) ferrites was carried out in the presence of citrate and nitrate using sol-gel self combustion method.[31] All high purity AR grade (99.99%) chemicals such as cobalt nitrate ($Co(NO_3)_2.6H_2O$), bismuth

nitrate ($Bi(NO_3)_2.5H_2O$), ferric nitrate ($Fe(NO_3)_3.9H_2O$) and citric acid ($C_6H_8O_7H_2O$) (sd-fine India) were used as received without purification. All reagents were weighted in stoichiometric proportions where metal nitrate to citrate ratio was 1:3. The cobalt and ferric nitrate were added in de-ionized water, bismuth nitrate was dissolved in concentrated hydrochloric acid. All solutions of nitrate salts were mixed together in a beaker of 1000 ml capacity. An aqueous solution of citric acid was mixed with metal nitrate solution as chelating agent at initial pH ~3. The pH of resulting solution was increased with an addition of ammonium hydroxide solution to ~7.[32] The beaker of solution was kept onto a hot plate while continuous stirring at 90°C. While evaporation; the solution changed to viscous and finally thick viscous gel. Subject to removal of all water molecules from the mixture, the gel was automatically ignited and burnt with glowing flints yielding ash. The decomposition reaction was continued until the whole citrate complex was consumed. The time required to complete the ignition was about one minute; yielding the black colored ash. We carried out these reactions for different concentrations (x = 0.0 to 0.2) of Bi^{3+}-doping so as to have $CoBi_xFe_{2-x}O_4$ ferrites. The as-prepared ferrites with different 'x' values were heat treated separately at 500°C for 4h to get impurity-free desired products. The phase-purity and crystal structure of these ferrites were examined through X-ray diffraction spectra, obtained on X-ray Rigaku–denki (Japan) diffractometer (D/MAX2500) with Cu-Kα radiation (λ =1.5418 Å) in the 2θ range from 20 to 70° with scanning rate 10°/min. The morphologies of as-developed ferrites were confirmed from the help of digital photo-images scanned on scanning electron microscopy (SEM) Hitachi S-4200. In later case, elemental proportions were corroborated from the energy dispersive X-ray (EDX) analysis. Fourier transformed infrared spectroscopy (FTIR; Shimadzu, Model 8400s) transmittance spectra were obtained in the wave number range of 4000-400 cm^{-1}. The magnetic measurements of $CoBi_xFe_{2-x}O_4$ ferrites were operated with a vibrating sample magnetometer (VSM; Lake Shore, Model 7404) at room temperature**.** The Mossbauer spectra were recorded at room temperature using $^{57}Co/Rh$ γ-ray source. The velocity scale was calibrated relative to ^{57}Fe in Rh. Recoil spectra analysis software was used for the qualitative evaluation of the Mossbauer spectra.

3. Results and discussion

3.1 Structural elucidation and morphological evolution studies

The XRD patterns of $CoBi_xFe_{2-x}O_4$ ferrites obtained for 0.0, 0.05, 0.1, 0.15 and 0.2 'x' values of Bi^{3+} –doping levels are shown in Fig. 1. XRD spectra confirm diffraction peaks of cubic spinel cobalt ferrite when 'x' is within $0 \leq x \leq 0.15$; which is in close agreement with 22-1086[33] JCPDS and also with literature.[34] Whereas, as Bi^{3+}-doping is increased i.e. when x = 0.2, additional peaks correspond to Bi_2O_3 (JCPDS card number 22-0515) are evolved. Presence of smaller and intense peaks in all XRD patterns is an indication of higher crystallinity, suggesting both doped and undoped ferrites were polycrystalline. The formation of secondary phase is due to electronic configuration and ionic radius of the trivalent Bi^{3+}. The Bi^{3+} of an ionic radius of ~1.03 Å, higher than that of Fe^{3+} (0.67 Å), occupies tetrahedral or octahedral sites more easily. Therefore, an excess substitution of Bi^{3+} leads to the formation of the secondary phase[35]. The micro-strain developed by substitution of Bi^{3+} decreases the lattice symmetry during the formation process and crystal imperfection. Distortion of strain induced peak broadening is related to micro-strain which is given by $\varepsilon = \beta_s/\tan\theta$. Crystallite size depends on diffraction angle θ, Scherrer equation follows $1/\cos\theta$ and Williamson Hall method follows $\tan\theta$. The crystallite and micro-strain both occur together due to the reflection broadening. Depending on different θ positions, the separation of size and strain broadening analysis was carried out using Williamson Hall method.[36] In this method, the XRD peak broadening is divided in two parts in accordance with $\beta_{hkl} = \beta_{size} + \beta_{strain}$ equation. The actual sample peak broadening is obtained by correcting the experimental peak broadening as $\beta^2 = \beta_P^2 - \beta_R^2$, where β_P is observed full-width at half maxima (FWHM) with the sample and β_R is FWHM of the peak of well-crystallites standard reference material. Therefore, original equation can be modified as;

$$\beta_{hkl} = \frac{0.9\,\lambda}{t\cos\theta} + 4\varepsilon\tan\theta \qquad 1$$

$$\beta_{hkl}\cos\theta = \frac{0.9\,\lambda}{t} + 4\varepsilon\sin\theta \qquad 2$$

where β- FWHM, ε- strain, λ- wavelength of X- ray, *t*- crystallite size.

It is assumed that strain is in all crystallographic direction $\beta\cos\theta$ (Y- axis) is plotted with respect to 4 $\cos\theta$ (X-axis). The micro-strain and crystallite size are calculated from the slope and Y axis-intercept of the fitted line, respectively. Fig. 2a shows the produced strain in $CoBi_xFe_{2-x}O_4$ ferrites. It is observed that the slope for pure $CoFe_2O_4$ is positive, indicating an existence of a small micro-strain in the lattice. The slopes for x = 0.05, 0.1, 0.15 $CoFe_2O_4$ products are negative; the amount of micro-strain must be very small. Slope for x = 0.2 ferrite is more positive, demonstrating larger micro-strain than $CoFe_2O_4$. This could be due to fact that the variation of Fe^{3+} between tetrahedral (A- site) and octahedral (B- site) increases since relatively bigger Bi^{3+} enter into the matrix of $CoFe_2O_4$ more easily. Variation of lattice constant '*a*' with Bi^{3+} -doping in $CoFe_2O_4$ is shown in (Fig. 2b) where lattice constant increases with Bi^{3+} substitution. The increase in lattice constant with Bi^{3+} addition is related to difference in ionic radii of Fe^{3+} and Bi^{3+}. The larger ionic radius of Bi^{3+} (1.03 Å) can replace smaller Fe^{3+} (0.67 Å) more easily which eventually increases the lattice constant could be due to swelling of unit cell dimension.[37] In the present system, increase in lattice constant with Bi^{3+}-doping obeys Vegard's law,[38] suggesting Bi^{3+}-doping is responsible for changing the structure of $CoFe_2O_4$. Presence of vacant lattice site at given composition is determined by a comparison of bulk density with the X-ray density. The X-ray density values are increased linearly with the Bi^{3+}-doping (Fig. 2 b).[39, 40]

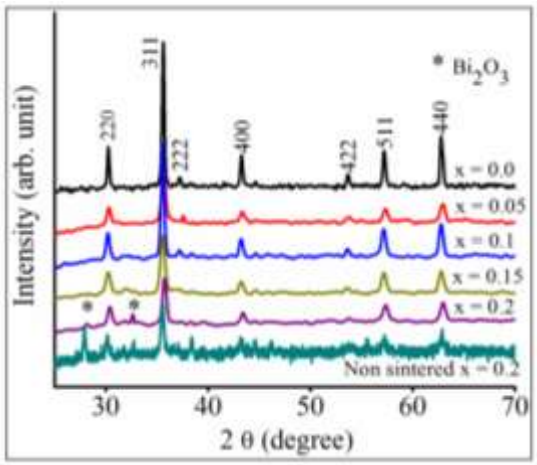

Fig. 1 The XRD patterns of $CoBi_xFe_{2-x}O_4$ (x = 0.0, 0.05, 0.1, 0.15 and 0.2) ferrites sintered in air at 500°C and non sintered for x=0.2.

Morphologies of $CoBi_xFe_{2-x}O_4$ ferrites were observed from digital SEM images. Fig. 3 (a-e) presents SEM images of $CoBi_xFe_{2-x}O_4$ ferrites for various 'x' values as a = 0, b = 0.05, c = 0.1, d = 0.15 and e = 0.20. Flat morphology with few air-voids is seen for $CoFe_2O_4$ ferrite (Fig. 3a). All crystallites are well-connected to one another in a relatively compact structure form. Valley and/or over growth are also noticed. Fig. 3b is the SEM image when 'x' is 0.05. Regular and polished crystallites are changed to irregular, rough and loose-type. For 'x' = 0.1 mol of Bi^{3+}, $CoFe_2O_4$ is agglomerated-type with some overgrowth which then is turned to flakes-type when 'x' is 0.15 mol of Bi^{3+}. For 'x'= 0.2 mol of Bi^{3+}, morphology is round-shape and scattered-type however, sphere-size is smaller than pristine $CoFe_2O_4$ (Fig. 2e). In short, surface of $CoFe_2O_4$ has been changed substantially with Bi^{3+}-doping from 0 to 0.2 mol. In ferrite structural, magnetic and electrical variation depends on exchange interactions of cation between octahedral and tetrahedral sites. In this study morphology changes with doping because substitution of Bi^{3+} enters tetrahedral (A) site and also octahedral [B] site for more Bi^{3+} concentration. Both tetrahedral and octahedral sites modify by Bi^{3+} causes change in the morphology with increasing grain growth[41].

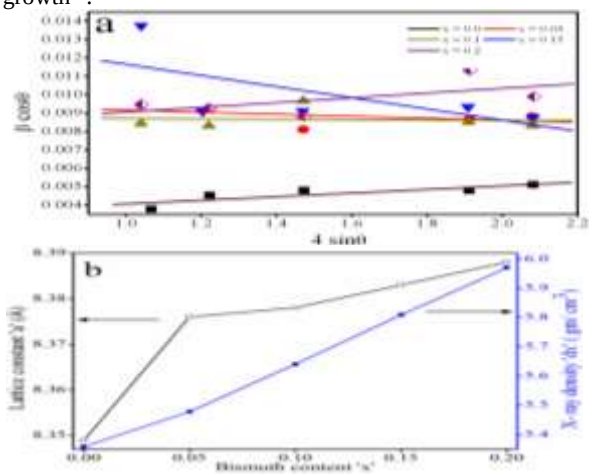

Fig. 2 (a) Williamson-Hall plots for $CoBi_xFe_{2-x}O_4$ ferrites, (b) variation of lattice constant '*a*' and X- ray density 'dx'with Bi content 'x'.

3.2 Elemental analysis

The EDX analysis of $CoBi_xFe_{2-x}O_4$ ($0 \le x \le 0.2$) ferrites was carried out for quantifying doping levels of Bi^{3+} in $CoFe_2O_4$. Fig. 4 shows the EDX spectrums of $CoFe_2O_4$ doped for various Bi^{3+} concentrations i.e. 0, 0.05, 0.10, 0.15 and 0.20. The O, Fe, Co, and Bi are major elements detected in ferrites except Bi in first i.e. $CoFe_2O_4$, indicating synthesized ferrites were pure in phase and Bi^{3+}-doping is successfully achieved. The estimated atomic percentages of O, Fe, Co, and Bi in pristine and doped $CoFe_2O_4$ ferrites are given in Table 1. The concentration of Co^{2+} is constant; indicating its proportion in ferrite structure is not responsible for both structural and morphological changes. However, the concentration of Bi is increased, demonstrating for Bi^{3+}-doping with Fe^{3+} in $CoFe_2O_4$ without disturbing Co^{2+}.

3.3 Fourier transforms infrared analysis

The FTIR spectra of $CoBi_xFe_{2-x}O_4$ ferrites obtained for 0.0, 0.05, 0.10, 0.15 and 0.20 'x' values were recorded in range of 4000-400 cm^{-1} (Fig. 5). The FTIR bands are assigned to vibrations of ions in crystal lattice and used for knowing the local symmetry in solids. The FTIR absorption bands are evolved due to vibrations of oxygen ions with metal cations.[42] Spinel ferrites reveal two metal-oxygen bands in FTIR spectra. The characteristics M-O absorption bands appeared at around 425-409 cm^{-1} (assigned to ν_1) and another at around 595-574 cm^{-1} (assigned to ν_2) are attributed to the presence of octahedral and tetrahedral sites, respectively.[43]

Table 1 Atomic percentage of O, Fe, Co and Bi in $CoBi_xFe_{2-x}O_4$ ferrites.

Bi^{3+} (mol) 'x'	O	Fe	Co	Bi	Total
0.0	44.71	34.7	20.59	0	100
0.05	48.29	32.23	18.59	0.89	100
0.10	36.95	39.81	21.9	1.34	100
0.15	39.56	37.38	20.71	2.35	100
0.20	42.43	34.85	19.41	3.3	100

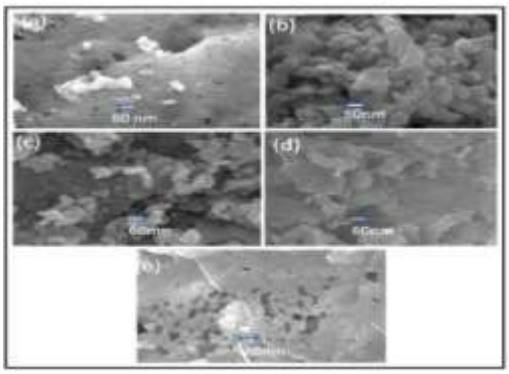

Fig. 3 The SEM images of $CoBi_xFe_{2-x}O_4$ ferrites for x = 0.0, 0.05, 0.1, 0.15 and 0.2.

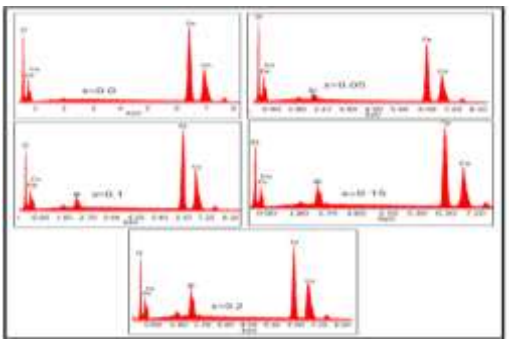

Fig. 4 EDX spectra of $CoBi_xFe_{2-x}O_4$ ferrites for x = 0.0, 0.05, 0.1, 0.15 and 0.2.

3.4 Mossbauer study

The ^{57}Fe Mossbauer spectra recorded at 300K for x = 0.0, 0.1, and 0.2 and fitted using available computer software is shown in Fig. 6. Mossbauer spectra exhibit normal magnetic sextet,[44] due

to Fe^{3+} on tetrahedral (A) site and other due to Fe^{3+} at octahedral [B] sites.

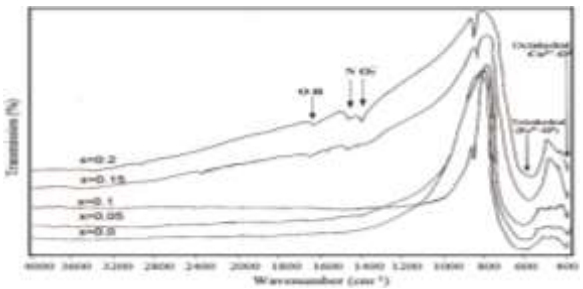

Fig. 5 FTIR spectra of $CoBi_xFe_{2-x}O_4$ ferrites for x = 0.0, 0.05, 0.1, 0.15 and 0.2.

The presence of a six line pattern in all spectra has confirmed magnetically ordered ferrite products.[45] Isomer shift (δ), quadrupole splitting (Δ), and hyperfine field (H_f) corresponding to tetrahedral (A) site and octahedral [B] site were obtained by curve-fitting process (WinNormos software).[46] The δ value at both (A) and [B] sites is same for x = 0.0 and 0.1, indicating the s-electron distribution of Fe^{3+} ions could be insensitive to the Bi^{3+} content. The δ value at (A) site is increased for x = 0.2, while at [B] site it is decreased with increasing non-magnetic Bi^{3+} content, which can be explained through the bonding nature of Fe^{3+} with Co^{2+} and Bi^{3+} at both sites.[47] With increasing 'x', Bi^{3+} can occupy both tetrahedral (A) and octahedral [B] sites. More number of Bi^{3+} can place in octahedral [B] site for x = 0.2 i.e. less migration of Fe^{3+} from (A) site to [B] site, the population of Fe^{3+} at (A) site can be increased while at [B] site it can be decreased.[17] Ions on [B] site with larger ionic radii and ions on (A) site with smaller ionic radii are responsible for the orbital overlapping. There is increased overlapping on [B] site and decreased overlapping on (A) site for smaller doping of Bi^{3+} ions. Due to which the δ value is decreased on [B] site and increased on (A) site. The H_f at the iron nucleus is proportional to saturation magnetization and is influenced by magnetic moment of ions and coupling with neighboring ions. In most of the cases, the H_f at the Fe^{3+} on [B] site is largest in the absence of non-magnetic neighboring ion and begins to decrease with increase of non-magnetic ion concentration.[48] Table 2 depicts decrease in H_f with Bi^{3+} ion concentration which is attributed to supertransferred hyperfine field components; strongly influenced by the superexchange coupling with neighboring ions and magnetic moments of these ions. Tetrahedral (A) site is occupied when Bi^{3+}-doping is increased, metal ions on octahedral [B] site create strong super-exchange interaction with neighboring (A) site ions, which is, in fact, a common behavior in spinel ferrites. It is observed that the value of H_f is decreased at both (A) site and [B] site with increasing non-magnetic Bi^{3+} concentration. Probability of the Fe^{3+} to find a Bi^{3+} as nearest neighbor may cause decrease in H_f. The Q value is an indication of the degree of deviation from cubic symmetric structure. The Q values of all $CoBi_xFe_{2-x}O_4$ ferrites are given in Table 2. There is no obvious variation in Q value, indicating Fe^{3+}, Co^{2+} and Bi^{3+} symmetry is unchanged between Fe^{3+} and their surrounding with addition of Bi^{3+} in the system.

3.5 Magnetic study

The variation of magnetization, M (emu/g) with applied magnetic field, H for $CoBi_xFe_{2-x}O_4$ ferrites at room temperature is shown in Fig. 7. The magnetization curves demonstrate the change in magnetic behavior of $CoFe_2O_4$ with the Bi^{3+}-doping, corroborating incubation of Bi^{3+} into $CoFe_2O_4$ matrix. All ferrites possess the ferrimagnetic behavior at room temperature. The M_s, H_c, M_r and R (=M_r/M_s) values for doped and undoped $CoFe_2O_4$ ferrites were calculated from the magnetization curves. The M_s value is increased with Bi^{3+}-doping level up to 0.10 and is then decreased when x ≥ 0.15. This can be explained by the fact that the ferrites follow Neel's two sub-lattices model.[49]

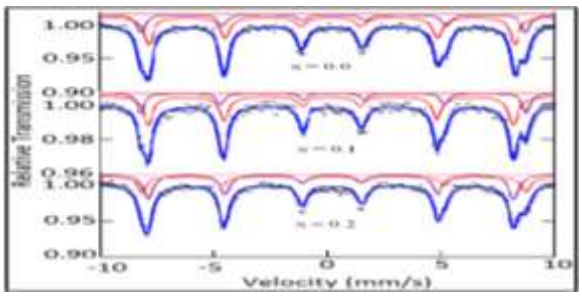

Fig. 6 Mössbauer spectra of $CoBi_xFe_{2-x}O_4$ ferrites for x = 0.0, 0.1, and 0.2.

According to Neel's model, the magnetic moment per formula unit is given by $n_B = M_B - M_A$, where M_B and M_A are the [B] and (A) sub-lattice magnetic moments in μ_B.

Table 2 IS, Q and H_{hf} values for (A) and [B] sites and n_B values, obtained from Mossbauer spectra.

Bi^{3+} (mol) 'x'	IS_A (mm/s)	IS_B (mm/s)	Q_A	Q_B	H_{hfA} (kOe)	H_{hfB} (kOe)
0.0	0.27	0.29	-0.008	-0.008	52.1	54.3
0.1	0.27	0.29	-0.008	-0.008	50.1	52.2
0.2	0.29	0.27	-0.008	-0.008	50.1	51.7

The Neel's magnetic moment was calculated by taking ionic magnetic moment of Co^{2+} ($3\mu_B$), Fe^{3+} ($5\mu_B$) and Bi^{3+} ($0\mu_B$).[50] The magnetization depends on cation distribution in (A) and [B] sites. The M_s is increased with increasing doping of Bi^{3+}, suggesting addition of non-magnetic Bi^{3+} preferred tetrahedral (A) site by replacing Fe^{3+} from (A) site to [B] site through diluting the magnetic moment of (A) site. The net magnetization, being difference between [B] and (A) sub-lattice, is increased due to increase in Fe^{3+} on [B] site. When substitution of Bi^{3+} is increased, Bi^{3+} prefers both tetrahedral (A) site and octahedral [B] site and there may be less migration of Fe^{3+} from (A) site to [B] site which eventually decrease the magnetic moment of [B] site and thereby M_s; can be the main reason for decreasing magnetization for x ≥ 0.15. The H_c value is increased up to x = 0.05 and then is decreased for more values of 'x', mainly depending upon the size of crystallite, domain structure and anisotropy of crystal structure.[51] Initially coercive field is increased for x = 0.05 because of formation of nanocrystalline structure and incorporation of Bi^{3+} into $CoFe_2O_4$ whereas, for x > 0.05, it is minimized due to decrease in anisotropy. This determines the difficulty of the magnetization direction away from its stable alignment with the preferred axis can find one of the influencing factors for magnitude of coercivity. The H_c is

decreased from 2446G to 1793G with Bi^{3+}-doping could be due an anisotropy change. Figure R is the characteristic parameter of the magnetic material. High R value is needed for magnetic recording and memory devices,[52] and provides an information with which the direction of magnetization reorients to nearest easy axis magnetization direction after the magnetic field is switched off. Lower value of the R, in the present case, is an indication of isotropic nature of $CoBi_xFe_{2-x}O_4$ ferrites. It is observed that the values of R are in range of 0.55 to 0.57, showing increasing trend with Bi^{3+} doping.

Table 3 M_s, H_c, M_r and R values of Bi-doped $CoFe_2O_4$ ferrites.

Bi^{3+} 'x'	M_s (emu g^{-1})	H_c (Oe)	M_r (emu g^{-1})	R= M_r/M_s
0	26.36	1457	14.48	0.55
0.05	37.55	2446	21.54	0.57
0.1	44.96	1863	24.63	0.55
0.15	37.01	1860	21.19	0.57
0.2	20.6	1793	11.53	0.56

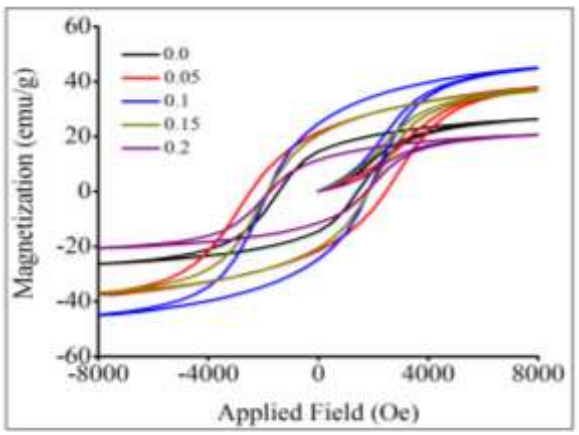

Fig 6 Magnetic hysteresis loops of $CoBi_xFe_{2-x}O_4$ ferrites.

4. Conclusions

We have successfully synthesized $CoBi_xFe_{2-x}O_4$ ferrites for various 'x' values from 0.0 to 0.2 using sol-gel self-combustion method followed by air-annealing at 500°C for 4 h. The XRD spectra have confirmed the formation of face-centered cubic spinel cobalt ferrite and moreover, the morphology is a function of Bi^{3+}-doping level. The lattice parameter and X-ray density are increased with Bi^{3+} i.e. with 'x'. Systematic increment of Bi^{3+} doping level is confirmed from the EDX measurement. Ferrimagnetism in doped and undoped $CoFe_2O_4$ ferrites is supported by the Mossbauer spectra. The isomer shift is increased at (A) site while decreased at [B] site. Up to x = 0.1 there is decrease in the hyperfine field which again is increased for x = 0.2. The quadrupole splitting for entire system shows no obvious variation. In magnetic study, saturation magnetization is increased with Bi^{3+}-doping up to x = 0.1 and then is again decreased for $x \geq 0.15$. The coercive field is increased up to x = 0.05 and then decreased with Bi^{3+}-doping level and finally, remanent ratio is in range of 0.55 to 0.57. These results corroborate favorable change in magnetic behavior of $CoFe_2O_4$ when doped with Bi^{3+} in different proportions and find potentiality in magnetic recording and memory devices.

Acknowledgements

This work is supported by the Global Frontier R&D Program (2013-073298) on Center for Hybrid Interface Materials (HIM) funded by the Ministry of Science, ICT & Future Planning. Authors (R.S. Mane, Mu. Naushad and Z.A Alothman) also extend their gratitude to the Visiting Professor (VP) Unit of King Saud University (KSU) and Deanship of Scientific Research, College of Science Research Center for the financial support. Authors are thankful to CIF Pondicherry University, Pondicherry for making VSM facility available.

References

1 W. Hu, N. Qin, G. Wu, Y. Lin, S. Li, D. Bao, *J. Am. Chem. Soc.*, 2012, **134**, 14658.
2 R. Ji, C. Cao, Z. Chen, H. Zhai, J. Bai, *Chem C.*, 2014, **2**, 5944.
3 N. Lee, T. Hyeon, *Chem. Soc. Rev.*, 2012, **41**, 2575.
4 J. Y. C. Chen, J. T. Miller, J. B. Gerkena, S. S. Stahl, *Energy. Env. Sci.*, 2014, **7**, 1382.
5 B. Li, H. Cao, J. Shao, M. Qub, J. H. Warner, *J. Mater. Chem.*, 2011, **21**, 5069.
6 A. Goldmen, in *Modern ferrite technology*, Springer, II Ed, 2006.
7 M. Hashim, Alimuddin, S. Kumar, S. E. Shirsath, R. K. Kotnala, J. Shah, R. Kumar, *Mater. Chem. Phys.*, 2013, **139**, 236.
8 A. A. Ati, Z. Othaman, A. Samavati, *J. Mole. Struct.*, 2013, **1052**, 177.
9 C. M. B Henderson, J. M Charnock, D. A Plant. *J. Phys: Condens. Matter*., 2007, **19**, 076214.
10 S. Jauhar, A. Goyal, N. Lakshmi, K. Chandra, S. Singhal, *Mater. Chem. Phys.*, 2013, **139**, 836.
11 S. M. Patange, S. E. Shirsath, G. S. Jangam, K. S. Lohar, S. S. Jadhav. *J. Appl. Phys.*, 2011, **109**, 053909.
12 J. Chand, G. Kumar, P. Kumar, S. K. Sharma, M. Knobel, M. Singh. *J. Alloy. Comp.*, 2011, **509**, 9638.
13 X. Wu, H. Yu, H. Dong, L. Geng. *Ceram. Int.*, 2014, **40**, 5905.
14 L. Kumar, M. Kar, *J. Magn. Mag. Mater.*, 2011, **323**, 2042.
15 Y. Yang, X. Liu, Y. Yang, W. Xiao, Z. Li, D. Xue, F. Li, J. Ding, *J. Mater, Chem. C.*, 2013, **1**, 2875.
16 M. Rahimi, M. Eshraghi, P. Kameli, *Ceram. Int*., 2014, **40**, 15569.
17 S. Verma, J. Chand, K. M. Batoo, M. Singh, *J. Alloy. Comp*., 2013, **565**, 148.
18 M. Sedlacik, V. Pavlinek, P. Peer, P. Filip, *Dalton. Trans.*, 2014, **43**, 6919.
19 C. Borgohain, K. K. Senapati, D. Mishra, K. C. Sarma, P. Phunkan, *Nanoscale.*, 2010, **2**, 2250.
20 R. Ji, C. Cao, Z. Chen, H. Zhai, J. Bai, *J. Mater. Chem. C.*, 2014, **2**, 5944.
21 C. Fernandes, C. Pereira, M. P. Fernandez-Garcia, *J. Mater, Chem. C.*, 2014, **2**, 5818
22 A. L. Rondinone, A. C. S. Samia, Z. J. Zhang, *J. Appl. Phys*., 2000, **76**, 3624.
23 A. S. Ponce, E. F. Chagas, R. J. Prado, C. H. M. Fernandes, A. J. Teezo, S. E. Baggio, *J. Magn. Mag. Mater.*, 2013, **344**, 182.
24 A. M. Kumar, K. H. Rao, J. M. Greneche., *J. Appl. Phys*., 2009, **105**, 073919.
25 D. Zhao, X. Wu, H. Guan, E. Han, *J. Supercrit. Fluids.*, 2007, **42**, 226.

26 S. Singhal, S. Jauhar, N. Lakshmi, S. Bansal, *J. Mole. Struct.*, 2013, **1038**, 45.
27 D. Varshney, K. Verma, *Mater. Chem. Phys.*, 2013, **140**, 412.
28 K. Verma, A. Kumar, D. Varshney, *Cur. Appl. Phys.*, 2013, **13**, 467.
29 M. A. Gabal, A. M. Abdel-Daiem, Y. M. Al Angari, I. M. Ismail, *Polyhedron*., 2013, **57**, 105.
30 A. Franco, F. L. A. Machado, V. S. Zapf, F. Wolff-Fabris, *J. Appl. Phys*., 2011, **109**, 07A745.
31 R. D. Purohit, A. K. Tyagi, *J. Mater. Chem*., 2002, **12**, 312.
32 I. Szczygiel, K. Winiarska, A. Bienko, K. Suracka, D. Gaworska-Koniarek, *J. Alloys. Comp.*, 2014, 604, 1.
33 C. Fei, Y. Zhang, Z. Yang, Y. Liu, R. Xiong, J. Shi, X. Ruan, *J. Magn. Mag. Mater.*, 2011, **323**, 1811.
34 Y. M. Abbas, S. A. Mansour, M. H. Ibrahim, S. E. Ali, *J. Magn. Mag. Mater.*, 2011, **323**, 2748.
35 S. E. Shirshat, M. L. Mane, Y. Yasukawa, X. Liu, A. Morisako, *Phys. Chem. Chem. Phys.*, 2014, **16**, 2347.
36 C. Pereira, A. M. Pereira, C. Fernandes, M. Rocha, R. Mendes, M. P. Fernandez-Garcia, A. Guedes, P. B. Tavares, J. M. Greneche, J. P. Araujo, C. Freire. *Chem. Mater*., 2012, **24**, 1496.
37 A. B. Gadkari, T. J. Shinde, P. N. Vasambekar, *Mater. Chem. Phys.*, 2009, **114**, 505.
38 S. A. Jadhav, Mater. *Chem. Phys.*, 2000, **65**, 120.
39 A. K Nikumbh, R. A. Pawar, D. V. Nighot, G. S. Gugale, M. D. Sangale, M. B. Khanvilkar, A. V. Nagawade, *J. Magn. Mag. Mater*, 2014, **355**, 201.
40 S. M. Hoque, M. S. Ullah, F. A. Khan, M. A. Hakim, D. K. Saha, *Phys. B.*, 2011, **406**, 1799.
41 L. Jia, H. Zhang, X. Wu, T. Li, H. Su, B. Liu, *J. Appl. Phys*., 2012, **111**, 07A326.
42 B. G. Toksha, S. E. Shirsath, M. L. Mane, S. M. Patange, S. S. Jadhav, K. M. Jadhav, *J. Phys. Chem. C.*, 2011, **115**, 20905.
43 E. Pervaiz, I. H. Gul, *J. Magn. Mag. Mater.*, 2012, **324**, 3695.
44 A. Ghasemi, V. Sepelak, X. Liu, A. Morisako, *J. Appl. Phys.*, 2010, **107**, 09A743.
45 A. M. Kumar, K. H. Rao, J. M. Greneche, *J. Appl. Phys.*, 2009, **105**, 073919.
46 Z. Z. Lazarevic, C. Jovalekic, A. Milutinovic, D. Sekulic, V. N. Ivanovski, A. Recnik, B. Cekic, N. Z. Romcevic, *J. Appl. Phys.*, 2013,**113**, 187221.
47 S. W. de Silva, F. Nakagomi, M. S. Silva, A. Franco Jr, V. K. Garg, A. C. Oliveira, P. C. Morais, *J. Appl. Phys.*, 2010, **107**, 09B503.
48 D. Yang, L. K. Lavoie, Y. Zhang, Z. Zhang, S. Ge, *J. Appl. Phys.*, 2003, **93**, 7492.
49 S. S. Jadhav, S. E. Shirsath, S. M. Patange, K. M. Jadhav, *J. Appl. Phys.*, 2010, **108**, 093920.
50 P. Priyadharsini, A. pradeep, P. S. Rao, G. Chandrasekaran, *Mater. Chem. Phys.*, 2009, **116**, 207.
51 A. S. Ponce, E. F. Chagas, R. J. Prado, C. H. M. Fernandes, A. J. Terezo, S.E. baggio, *J. Magn. Mag. Mater.*, 2013, **344**, 182.
52 U. B. Shinde, S. E. Shirsath, S. M. Patange, S. P. Jadhav, K. M. Jadhav, V. L. Patil, *Ceram. Int.*, 2013, **39**, 5227.